Published in final edited form as:
Photochem Photobiol Sci. 2011 May ; 10(5): 832–841. doi:10.1039/c1pp05022b.

Methylene blue covalently loaded polyacrylamide nanoparticles for enhanced tumor-targeted photodynamic therapy†

Ming Qin[a], **Hoe Jin Hah**[a], **Gwangseong Kim**[a], **Guochao Nie**[a,b], **Yong-Eun Koo Lee**[a], and **Raoul Kopelman**[a]

Raoul Kopelman: kopelman@umich.edu

[a]Department of Chemistry, University of Michigan, 930 N. University, Ann Arbor, Michigan, 48109, USA.; Fax: +1 734 976 2778; Tel: +1 734 764 7541

[b]Department of Chemistry and Biology, Yulin Normal University, Yulin City, Guangxi, 537000, China

Abstract

The use of targeted nanoparticles (NPs) as a platform for loading photosensitizers enables selective accumulation of the photosensitizers in the tumor area, while maintaining their photodynamic therapy (PDT) effectiveness. Here two novel kinds of methylene blue (MB)-conjugated polyacrylamide (PAA) nanoparticles, MBI-PAA NPs and MBII-PAA NPs, based on two separate MB derivatives, are developed for PDT. This covalent conjugation with the NPs (i) improves the loading of MB, (ii) prevents any leaching of MB from the NPs and (iii) protects the MB from the effects of enzymes in the biological environment. The loading of MB into these two kinds of NPs was controlled by the input amount, resulting in concentrations with optimal singlet oxygen production. For each of the MB-NPs, the highest singlet oxygen production was found for an MB loading of around 11 nmol mg^{-1}. After attachment of F3 peptide groups, for targeting, each of these NPs was taken up, selectively, by MDA-MB-435 tumor cells, *in vitro*. PDT tests demonstrated that both kinds of targeted NPs resulted in effective tumor cell kill, following illumination, while not causing dark toxicity.

Introduction

Photodynamic therapy (PDT) is gaining increasing recognition as a medical treatment for cancer, especially skin cancer, and for other dermatological problems, such as acne, as well as for macular degeneration. This treatment uses PDT drugs (called photosensitizers), in combination with light, to kill selected cells. It relies on the generation of singlet oxygen and other kinds of reactive oxygen species (ROS), causing cell death by apoptosis, necrosis and/or autophagy.[1] The first clinical PDT treatment was approved in the US in 1995.[2] Since then, PDT has been approved for the treatment of skin actinic keratosis, several forms of cancer, blindness due to age-related macular degeneration, *etc.*[3–5] PDT is a localized treatment, selectively activated by light, and thus causing low systemic toxicity. It can be applied by itself or in combination with other treatment methods, *e.g.*, chemotherapy and surgery.[6]

An ideal photosensitizer for PDT should have a stable composition, photostability, minimum dark toxicity, high absorption in the red or near infrared region of the spectrum, reasonable hydrophilicity, target specificity, and quick clearance from the body.[7] Many kinds of

†This article is published as part of a themed issue on immunological aspects and drug delivery technologies in PDT.

Correspondence to: Raoul Kopelman, kopelman@umich.edu.

photosensitizers have been developed so far. However, very few of them satisfy those requirements. Methylene blue (MB), a hydrophilic phenothiazine derivative,[8–10] has been used as a drug in clinical applications for malaria and methemoglobinemia.[11,12] MB has also been approved as a potent PDT drug for local treatment of periodontal diseases (Periowave, Canada), because of its relative low toxicity and high generation yield of singlet oxygen.[13,14] MB exhibited phototoxicity towards a variety of tumor cell lines *in vitro*.[9,15] Combined with illumination, MB was reported to cause 75% destruction of human colon tumor xenografts.[16] Also the local administration of MB intralesionally had some success with recurrent inoperable esophageal cancer in three patients.[17]

Some drawbacks of MB have limited its further clinical application as a PDT agent. The activity of MB became relatively low when injected intravenously or intravesically, which was attributed to poor tumor localization.[9,13] In addition, the methylene blue photosensitizer is converted to its leuko- (colorless) isomer in the biological environment, a non-photosensitizer with negligible photodynamic activity.[18] This MB reduction is catalysed by either NADH/NADPH dehydrogenases within the cell or transmembrane thiadizine dye reductase at the cell surface.[11,19]

In order to improve the performance of photosensitizers, they should be targeted specifically to the tumor cells. This can be achieved by embedding them inside a nanoparticle (NP) and attaching a targeting group on the periphery of the particle, *e.g.*, antibodies or tumor-specific peptides. For instance, F3 peptide, a 31-amino acid peptide, is known to bind to the angiogenic tumor vasculatures, as well as to some tumor cells, by interacting with nucleolin, a cell surface receptor.[20,21] The effect of enhanced permeability and retention (EPR) of NPs can also improve the local distribution of photosensitizers.[22] The nanoparticle matrix has to be porous to the outgoing singlet oxygen.[23] The design concept of NP-based PDT was first introduced in 2000 and the *in vivo* performance was demonstrated subsequently.[24–28] We note that for drugs such as MB that can be inactivated by plasma enzymes[23,29–31] a protective carrier system is necessary, *e.g.*, the nanoparticle matrix.[32] As a drug carrier, the advantages of NPs also include good solubility, high loading of drugs and alleviating the multidrug resistance effect of cancer cells.[31,33]

The polyacrylamide (PAA) nanoparticle, due to its ideal size, biocompatibility and hydrophilicity, has been used for *in vivo* cancer imaging and treatment.[24–27] MB has been loaded in PAA NPs by encapsulation or by covalent linkage, exhibiting phototoxicity in a variety of cancer cell lines *in vitro*.[23,32,34–37] The encapsulation method resulted in low dye loading and the MB-encapsulated NPs required prolonged PDT illumination time or high dose for cell kill. Moreover, the encapsulated MB may leach out of the NPs. In our previous studies, MB was conjugated into PAA NPs *via* a two-step reaction (MBSE-PAA NPs).[37] This conjugation method prevented the drug leaching phenomena, increased significantly the loading of MB, and improved the singlet oxygen production of the NPs. The singlet oxygen production, which is a critical parameter of MB-conjugated PAA NPs for PDT, is controlled largely by the structure of the MB derivative and by its loading into the NPs.[9,37] One question we were interested in about MB-PAA NPs is whether better singlet oxygen production of the NPs can be obtained by varying the MB derivatives and their loading into the NPs. Recently, two new kinds of MB derivatives (see Scheme 1 for their chemical structures), 3,7-bisallylmethylene blue (MBI) and 3,7-bismethylacrylamide methylene blue (MBII), were synthesized in our lab (The synthetic details will be reported separately). In the work reported here, MBI and MBII were conjugated into PAA NPs *via* a one-step reaction. For both MBI-PAA NPs and MBII-PAA NPs, the loading was controlled by the amount of MB derivatives that were added before polymerization. We report below the relationship between MB loading and singlet oxygen production for both kinds of MB-conjugated NPs, as well as the optimal singlet oxygen production. We compare the singlet

oxygen production of MB-encapsulated NPs, MBSE-PAA NPs, MBI-PAA NPs and MBII-PAA NPs. We also show that this NP matrix protects the conjugated MB from the reduction by diaphorase (NADH dehydrogenase), while maintaining its photodynamic activity. The MBI-PAA NPs and MBII-PAA NPs were surface-conjugated with F3 peptide targeting groups for PDT specific to selected tumor cells.[37] The *in vitro* PDT experiments show that both kinds of NPs, when combined with illumination, are capable of killing MDA-MB-435 cancer cells effectively. We believe that our work reported here may further the application of MB for photodynamic therapy.

Experimental

Materials

3,7-Bisallylmethylene blue (MBI) and 3,7-bismethylacrylamide methylene blue (MBII) were synthesized in our lab. Acrylamide (AA), glycerol dimethacrylate (GDMA, 85%), ammonium persulfate (APS), *N,N,N′,N′*-tetramethylethylenediamine (TEMED), sodium dioctyl sulfosuccinate (AOT), Brij 30, dimethylformamide (DMF), dimethylsulfoxide (DMSO), phosphate-buffered saline tablet (PBS), β-nicotinamide adenine dinucleotide, reduced dipotassium salt (NADH), diaphorase from *Clostridium kluyveri* (NADH dehydrogenase) and 3-(4,5-dimethylthiazolyl-2)-2,5-diphenyltetrazolium bromide (MTT) were purchased from Sigma Aldrich. *N*-(3-Aminopropyl)methacrylamide hydrochloride (APMA) was purchased from Polysciences. Anthracene-9,10-dipropionic acid disodium salt (ADPA), calcein acetoxymethyl ester (calcein AM) and propidium iodide (PI) were purchased from Invitrogen. Ethanol (95%) and hexane were purchased from Fisher Scientific. F3-Cys peptide (KDEPQRRSARLSAKPAPPKPEPKPKKAPAKKC) was purchased from SynBioSci. The MAL-PEG-SCM (2 K) (SCM: succinimidyl carboxy methyl ester, one type of NHS ester) was purchased from Creative PEGWorks. All the water used was purified with a Milli-Q system from Millipore.

Preparation of MB-conjugated PAA NPs

MBI-PAA NPs and MBII-PAA NPs were synthesized with a reverse microemulsion polymerization method (in Scheme 2). Deoxygenated hexane (45 mL), AOT (1.95 g) and Brij 30 (4.9 mL) were mixed together, and the mixture was stirred vigorously to produce a microemulsion. AA (610 mg), APMA (45 mg), GDMA (403 mg) and MBI or MBII were dissolved in DI water (1.2 mL) directly. The amount of MB added ranged from 10 mg to 90 mg, depending on the required loading of MB. The solution was sonicated until dissolved completely. Then the monomer solution was added into the hexane solution under argon atmosphere for 20 min. Fresh APS solution (200 μL, 50% w/v) and TEMED (150 μL) were added into the mixture solution to initiate polymerization. After 2 h reaction, hexane was removed by rotary evaporation. The residue was suspended in ethanol and transferred into an Amicon ultra-filtration cell (Millipore Corp.). In order to remove the surfactants and unreacted monomers, the NPs were washed with ethanol and DI water respectively with a 300 kDa filter membrane under the pressure of 15–20 psi. This washing process was repeated five times. After filtration with 0.2 μm filter PTFE membrane (Whatman), the NPs were lyophilized and stored in freezer. The loading of MB in the NPs was controlled by the amount of MB added in.

Characterization

The loading of MB in the NPs was evaluated by taking absorption spectra of the MB-conjugated PAA NP suspensions in DI water (1 mg mL^{-1}) with a UV-1601 UV-vis spectrometer (Schimadzu). The fluorescence spectra of MB-conjugated NP suspension in PBS buffer (0.3 mg mL^{-1}) were taken with a FluoroMax-3 Spectrofluorometer (Jobin Yvon Horiba). Scanning electron microscopy (SEM) images of NPs were obtained with an FEI

Nova Nanolab dualbeam focussed ion beam workstation and scanning electron microscope. The sample for SEM analysis was prepared as follows: (1) NP solution (0.1 mg mL^{-1}) was sonicated for 30 min to make sure the NPs were dispersed completely; (2) a drop of NP solution was placed on the SEM specimen mount and dried completely under room temperature; (3) then the sample was coated with gold before SEM analysis. The size and zeta potential of NPs in aqueous solution (1 mg mL^{-1}) were measured using dynamic light scattering (DLS) with Delsa Nano (Beckman Coulter) instrument.

Dye leaching test

A MB-PAA NP solution (1 mL, 1 mg mL^{-1}) was mixed with a bovine serum albumin (BSA) solution (1 mL, 4%). The mixture solution in PBS buffer (pH 7.4) was stirred at 37 °C for 1.5 h. After that, the solution was diluted to 8 mL in PBS buffer (pH 7.4) and transferred to an Amicon ultra-filtration cell (Millipore Corp.). The solution was filtered with filter membrane (300 kDa) till the filtrate was 5 mL. Then a PBS buffer (5 mL, pH 7.4) was added to the Amicon ultra-filtration cell and this filtering process was repeated for 3 times. The filtrates (5 mL) 1, 2 and 3 were collected respectively. The fluorescence emission intensity was measured with FluoroMax-3 Spectrofluorometer (Jobin Yvon Horiba).

F3 peptide attachment to MB-conjugated NPs

MAL-PEG-SCM (4 mg) was added into a MB-conjugated PAA solution (2.5 mL, 20 mg mL^{-1}, PBS (pH 7.4)), and the solution was stirred for 30 min at room temperature. Then the NP solution was transferred to an Amicon centrifugal filter (100 kDa). The NP solution was rinsed with centrifugation at 4000 *g* for 20 min. After 3 times washing, the NP solution was concentrated to be around 20 mg mL^{-1}, and mixed with an F3-Cys peptide solution (110 μL, 100 mg mL^{-1}) under stirring. After stirring overnight, the NP solution was rinsed with centrifugation for 3 times and collected at 20 mg mL^{-1}. Then the NP solution was mixed with an L-cysteine solution (63 μL, 10 mg mL^{-1}). After 2 h reaction, the NP solution was washed with centrifugation for 3 times and collected at 20 mg mL^{-1}. The amount of peptides conjugated on the NPs was determined by quantitative amino acid analysis (QAAA).

PEGylation of MB-conjugated NPs

MAL-PEG-SCM (4 mg) was added into a MB-conjugated PAA solution (2.5 mL, 20 mg mL^{-1}, PBS (pH 7.4)), and the solution was stirred for 30 min at room temperature. After that, the NP solution was transferred to an Amicon centrifugal filter (100 kDa). The NP solution was rinsed with centrifugation at 4000 *g* for 20 min. After 3 times washing, the NP solution was concentrated to be around 20 mg mL^{-1}, and mixed with an L-cysteine solution (125 μL, 10 mg mL^{-1}). After 2 h reaction, the NP solution was washed with centrifugation for 3 times and collected at 20 mg mL^{-1}.

Singlet oxygen detection

The generation of singlet oxygen ($^1O_2$) from MB-conjugated PAA NPs was determined by the ADPA method.[23,38] An MB-conjugated PAA NP solution (2 mL) in PBS buffer (0.3 mg mL^{-1}) was mixed with an ADPA solution (80 μL, 100 μM) in a 4 mL-cuvette. The solution was illuminated at 660 nm with a slit width of 10 nm with a 150 W ozone-free xenon-arc lamp. The actual power illuminated on the sample was around 2 mW. After illumination at different time scales (0, 1, 3, 5, 10, and 15 min), the fluorescence emission spectra of ADPA were collected under the excitation at 378 nm.

In this method, ADPA reacts with $^1O_2$ and generates ADPA endoperoxide. The decay of [ADPA] follows first order kinetics if the rate of deactivation of $^1O_2$ by reaction with ADPA is neglibile compared to the deactivation by the solvent:[38]

$$\ln\left(\frac{[\mathrm{ADPA}]_t}{[\mathrm{ADPA}]_0}\right) = -kt \quad (1)$$

$$k = k_c[^1O_2] = \varphi^{^1O_2} I^{abs} \frac{k_c}{k_d} \quad (2)$$

Where k_c is the rate constant of chemical quenching of $^1O_2$ by ADPA, and k_d is the decay rate of $^1O_2$ to $^3O_2$ by energy transfer to the solvent or to other species in solution. $\varphi^{1}O_2$ is the generation efficiency of $^1O_2$ of a photosensitizer, and I^{abs} is the rate of photo absorption.

Here, the rate constant k is an indicator of singlet oxygen efficiency, $\varphi^{1}O_2$.

Enzymatic reduction test of MB

The enzymatic reduction of MB was tested by the method reported before.[32] An aliquot of MB, MBI or MBII solution (3 mL, 3 μM) in PBS buffer (pH 7.4) was mixed with NADH (0.45 μmol) and diaphorase (0.05 mg). The fluorescence intensity of MB at 680 nm in the mixed solution was measured for 1 h with a FluoroMax-3 Spectrofluorometer (Jobin Yvon Horiba). The MBI-PAA NP or MBII-PAA NP solution (0.3 mg mL^{-1}) was tested in the same way. As a control, the fluorescence intensity of these solutions without NADH and diaphorase was measured under the same condition for the photobleaching effect.

MTT assay

The dark toxicity of MBI-PAA NPs and MBII-PAA NPs was analyzed, using an MTT assay, for the human melanoma cell line MDA-MB-435. The cells were incubated with MBI-PAA NPs or MBII-PAA NPs (0.2 mg mL^{-1}) on 96-well plates, containing 5000 cells in each well, for 1 h before testing with the MTT assay. The cells were treated with an MTT reagent (0.5 mg mL^{-1}) for an additional 4 h. Then, the produced formazan crystals were solubilized in DMSO overnight. The visible absorption from each well was measured at 550 nm in a Biochrom Anthos microplate reader.

In vitro targeting and photodynamic tests

The human melanoma cell line MDA-MB-435 was incubated with F3-targeted MB-PAA NPs (F3-MB-PAA NPs, 0.1 mg mL^{-1}) or PEGylated MB-PAA NPs (PEG-MB-PAA NPs, 0.1 mg mL^{-1}) for 15 min on the cover slips, cultivated in 6-well cover plates. Then the tumor cells were washed with cell culture media three times to remove the unbound NPs. The fluorescence images of the cells were taken using a 647 nm laser with 400 μW of power (exposure time: 0.2 s) and analyzed for cellular NP uptake by a Perkin Elmer Ultra View Confocal microscope system equipped with an argon-krypton laser. Calcein AM (0.4 μM) and PI (7 μM) were then added into cells and PDT was performed on cells with the same light source but with 1 min illumination (*ca.* 100 J cm^{-2}). After 20 min, the fluorescence staining images of calcein AM and PI were taken. The excitation wavelength and emission wavelength of calcein AM are 488 nm and 525 nm, respectively, while the excitation wavelength and emission wavelength of PI are 568 nm and 600 nm, respectively.

Results and discussion

Preparation and characterization of MB-conjugated PAA NPs

Two critical elements for the successful preparation of NPs are the ratio of organic phase/water/surfactants and the amount of initiators. The first one is related with the formation of the nanodroplets in the continuous phase, while the second one is related with the polymerization inside these droplets. Compared to the preparation conditions of blank PAA NPs,[39] the following two modifications were made for the MB-conjugated PAA NPs: (a) Higher than typically used amounts of initiators (25 times of APS and 4 times of TEMED) are required for the preparation of MB-conjugated NPs. (b) In order to avoid aggregation of NPs, higher amounts of surfactants (2 times of AOT and 1.5 times of Brij 30) are necessary while the amount of hexane and water are kept the same as before. In this reaction, AA is the main monomer, GDMA is a biodegradable cross linker, and APMA provides the amine groups, which can be used for NP modification. High amounts of initiators may result from partial quenching of free radicals by the higher amounts of surfactants, as well as by the MBI and MBII.

The spectral characteristics and the MB loading of the NPs were determined by both UV-vis spectroscopy and fluorescence spectroscopy, seen in Fig. 1(a) and 1(b). Compared to the absorption wavelength (652 nm) of the MBI solution, the absorption of MBI-PAA NPs is shifted to a longer wavelength (654 nm). Similarly, the absorption wavelength of MBII is also shifted from 654 nm in the MBII solution to 656 nm in the MBII-PAA NP solution. It should be noted that there is a noticeable peak at 610 nm in the absorption spectra of both MBI-PAA NPs and MBII-PAA NPs, in contrast to the absorption spectra of MBI solution and MBII solution. The presence of the 610 nm peak indicates formation of MB dimers inside the NPs,[40–42] probably due to the relatively high concentration of MB within the NPs. MB dimers were also formed at high concentrations of MB in aqueous solution (where there is no conjugation).[40] It is interesting to see that MB dimers were formed even when the MB derivative was covalently conjugated inside the NPs. MB aggregates, other than dimers, are not likely to occur as MB is conjugated to the NP polymeric matrix. The MB loading in the NPs was estimated based on the peak area between 420–800 nm, using the Beer–Lambert law. The loading of MB is correlated well with the amount of MB added in. The MBI loading ranges from 6.4 nmol mg^{-1} to 23.3 nmol mg^{-1} in the 5 batches of MBI-PAA NPs; while, for MBII-PAA NPs, the MBII loading ranges from 5.5 nmol mg^{-1} to 136.9 nmol mg^{-1}

The fluorescence excitation and emission spectra of the MBI and MBII-conjugated PAA NPs as well as MBI and MBII solutions are shown in Fig. 1(b). The excitation and emission peak wavelengths of the MBI-PAA NPs are at 663 nm and 680 nm, respectively, which are the same as those of the MBI solution. The excitation and emission wavelengths of the MBII-PAA NPs were also the same as those of the MBII solution (662 nm and 680 nm). The fluorescence intensities of MBI-PAA NPs and MBII-PAA NPs were a little weaker than those of MBI and MBII in solution, under the same dye concentration, which is probably due to the formation of more MB dimers, or self-quenching of MB within the NPs.

The formation and size of the NPs was tested by dynamic light scattering (DLS), as in Fig. 2(a). The DLS data showed that the size of the MBI-PAA NPs in the aqueous solution increased from 57 to 112 nm when the loading of MBI increased from 6.4 nmol mg^{-1} to 23.3 nmol mg^{-1}. Similarly, for MBII-PAA NPs, the size of NPs ranged from 30 to 99 nm when the MB loading ranged from 5.5 nmol mg^{-1} to 30.1 nmol mg^{-1}. This phenomenon demonstrates that under similar preparation conditions, the size of the NPs is influenced by the amount of MB per NP. The morphology of the MBI-PAA NPs (MBI loading: 11.0 nmol mg^{-1}) and MBII-PAA NPs (MBII loading: 10.4 nmol mg^{-1}) was also analyzed by SEM,

seen in Fig. 2(b) and 2(c). The average diameters of the MBI-PAA NPs and MBII-PAA NPs from SEM are 18.4 nm and 13.6 nm, respectively, compared to 74.4 nm of MBI-PAA NPs and 38.4 nm of MBII-PAA NPs in aqueous solution, respectively (from DLS). These results verified that the MB-PAA NPs in aqueous solution are larger than the size given by the SEM images, since hydrogel PAA NPs absorb water and swell in aqueous solution. Both MBI-PAA NPs and MBII-PAA NPs are very soluble in both DI water and PBS buffer, the solubility of which is around 100 mg mL^{-1} in PBS buffer. Additionally, these NPs were incubated with a BSA solution at 37 °C for 1.5 h, in order to test the leaching of MB out of the NPs. The spectral results in Fig. 3(a) and 3(b) show that no MB leached out from the NPs, which means that the covalent conjugation method practically prevents the PDT drug from leaching out of the NPs.

Singlet oxygen efficiency

The efficiency of photodynamic therapy relies on the $^1O_2$ production, which is represented by the *k* value in eqn (2). The *k* values of both MBI-PAA NPs and MBII-PAA NPs were tested by the ADPA method with the same NP concentration (0.3 mg mL^{-1}). Plotting the graph of $\ln([ADPA]_t/[ADPA]_0)$ *vs.* time, the *k* value is the slope of the curve, seen in Fig. 4.

We studied the relationship between the *k* value and the MB loading in both kinds of NPs, as shown in Fig. 5. For MBI-PAA NPs, when the drug loading increased, starting from 6.4 nmol mg^{-1}, the *k* value increased gradually to a maximum when the drug loading was about 11.0 nmol mg^{-1}; then, when the drug loading continued to increase from 11.0 nmol mg^{-1} to 23.3 nmol mg^{-1}, the *k* value decreased. This means that the optimal $^1O_2$ production from the MBI-PAA NPs was found at an MB loading of around 11.0 nmol mg^{-1}. The relationship between the *k* value and the drug loading of the MBII-PAA NPs showed a similar trend in which the *k* values increased with the MB loading up to 10.4 nmol mg^{-1} and then decreased. The highest *k* value for the MBII-PAA NPs was found for an MB loading of 10.4 nmol mg^{-1}. The phenomenon—a decrease of *k* values when the MB loading increases beyond an optimal loading—is most probably related to the dimerization of MB inside the NPs. As the MB loading increases, the ratio of MB dimers (absorption max at 610 nm) to MB monomers (absorption max at 655 nm), within the NPs, increases while the amount of MB monomer molecules per NP also increases (Fig. 6(a)). The $^1O_2$ production from the NPs relies on the amount of MB monomer molecules per NP. The k value of the MBII-PAA NPs appears to increase at a loading of 30.1 nmol mg^{-1}, compared to that at 14.0 nmol mg^{-1}, but this may not be significant due to the uncertainties (see error bars in Fig. 5). If real, this trend might be due to a higher absolute amount of MB monomer molecules in the NPs with dye loading of 30.1 nmol mg^{-1} (this is hard to tell due to the significant spectral overlap of monomer and dimer absorption peaks, Fig. 6(a)). We note that at the higher loading, the self-quenching of MB excited states must also increase (see relative increase in dimer absorption peak, Fig. 6(a)), and therefore the $^1O_2$ production at an MB loading of 30.1 nmol mg^{-1} is still less than that at 10.4 nmol mg^{-1}. The fluorescence intensity of MB, which also depends on the amount of MB monomer molecules per NP (Fig. 6(b)), shows a similar trend to that of the $^1O_2$ production (*k* values in Fig. 5), though, again, the fluorescence values for the 14.0 and 30.1 nmol mg^{-1} loadings are the same, within the error bars (see Fig. 6(b)).

We also compared the best *k* values for the MB-encapsulated PAA NPs, MBSE-PAA NPs, MBI-PAA NPs and MBII-PAA NPs (see Table 1). The MB-conjugated PAA NPs of all the preparations (MBSE-PAA NPs, MBI-PAA NPs and MBII-PAA NPs) resulted in better $^1O_2$ production than the MB-encapsulated NPs, which is primarily related with the higher loading of MB in the conjugated NPs. The $^1O_2$ production of MB-conjugated PAA NPs followed this order: MBI-PAA NPs >MBII-PAA NPs >MBSE-PAA NPs.

Enzymatic reduction of MB

Our group reported earlier that the encapsulation of MB into PAA NPs prevented the interaction of MB with enzymes and thus effectively maintained its photodynamic activity.[32]

In order to verify the hypothesis that the conjugation method can also largely prevent the MB from reduction by enzymes outside the NPs, the MB-PAA NP solution or MB solution was tested by the same method. When it was mixed with NADH and the diaphorase (24 kDa), the reduction of MB was confirmed by the decrease of fluorescence intensity of MB at 680 nm in both MB and MB-PAA NP solution. The temporal changes in the fluorescence emission intensity at 680 nm of the MB, MBI, MBII, MBI-PAA NP and MBII-PAA NP solutions are shown in Fig. 7. Over 80% decrease of fluorescence intensity was found for MB, MBI and MBII solution in 1 h. Howver, only a 30% and 50% decrease of fluorescence signal was found for MBI-PAA NP and MBII-PAA NP solutions, respectively. These results confirm that the PAA matrix helps, at least in part, to protect the dyes from the biological environment and to retain their photodynamic activities. The reason for this protection may be that the diaphorase can not penetrate into the NPs because of its large molecular size. However, part of MB conjugated on the particle surface was reduced by diaphorase. That is why the decrease of fluorescence intensity was still found for the MB-PAA NPs solution.

PEGylation and F3 attachment to MB-conjugated PAA NPs

In our previous studies, the F3-conjugated PAA NPs were demonstrated to have efficient binding to, internalization into, and, as a result, enhanced therapeutic efficiency toward tumor cell lines that express high levels of nucleolin on their cell surface, *e.g.* the MDA-MB-435 melanoma cell line and the 9 L glioma cell line, compared to tumor cell lines with low expression of nucleolin, *e.g.* the MCF-7 breast cancer cell line.[37,43,44] This targeting specificity was confirmed to depend on F3-nucleolin interactions, by comparing the targeting efficiency of NPs conjugated with F3 peptides and those of NPs with scrambled F3 peptides.[43] We have also shown that the F3-targeted PAA NPs can deliver efficiently diagnostic and/or therapeutic small molecules to glioma and ovarian tumor rodent models, enabling effective therapeutic outcomes.[28,39]

In order to prepare NPs that selectively target specific tumor cells, the PAA NPs were modified by attachment of the F3 peptides *via* a cross linker, MAL-PEG-SCM. The SCM groups from MAL-PEG-SCM react with the amine groups on the NP surface and generate amide groups, while the MAL groups react with the thiol groups of the F3 peptides and generate carbon-sulfur bonds. PEG was reported to improve the hydrophilicity of NPs and increase the circulation time of NPs in the body.[25,45] In order to test the targeting effect of F3-modified NPs, PEGylated NPs were used as a negative control. The QAAA results showed that the amount of F3 peptide attached on the NPs was 0.027 μmol per mg NPs.

The PEGylation and F3-peptide conjugation of the NPs were also monitored with the zeta potential test. Before modification, the zeta potential of MBII-PAA NPs was ~15.4 mV, because of the positive amine groups on the surface; after PEGylation, since most of the NP surface was covered with neutral PEG, the zeta potential of the NPs was close to neutral (~1.8 mV); after reaction with the F3 peptide, the whole NP surface became positively charged again (~8.6 mV), which is related with the cationic nature of the F3 peptide.

In vitro targeting and PDT

In order to verify the cell kill effects of the MB-conjugated NPs, *in vitro* PDT tests were performed on the MDA-MB-435 tumor cell line, which is known to express high levels of

nucleolin. The NPs with MB loadings around 11 nmol mg^{-1} were chosen for the *in vitro* PDT test because of their highest $^1O_2$ production.

The uptake of MB-PAA NPs by tumor cells was monitored *via* the fluorescence images of tumor cells, based on the MB fluorescence under the confocal microscope (Fig. 8). The NPs were incubated with the cells for 15 min—the optimal incubation time for sufficient specific binding but minimal nonspecific binding.[43] It was observed that the F3-MB-NPs accumulated in the cell membrane and cytoplasm after 15 min incubation, while the PEG-modified MB-NPs did not. These results are consistent with previous results published by our group.[37,44] Note that the light dose used for fluorescence imaging was not high enough to cause PDT effects on the cells—it was only 1/300 of the PDT dose (0.2 s *vs.* 1 min). The amount of F3-MB-NPs per cell was estimated to be ~6×10^{-8} mg per cell, based on the previously reported saturated amount of NPs per cell[44] and the current incubation condition that corresponds to ~40% saturation.[43]

The fluorescence images of the tumor cells treated with calcein AM and PI before and after PDT are shown in Fig. 9. Before illumination, both F3-MBI-NP-treated tumor cells and PEG-MBI-NP-treated tumor cells were alive (Fig. 9(a) and 9(b)). At 20 min after a 1 min illumination, almost all F3-MBI-NP-treated tumor cells were dead, while the PEG-MBI-NP-treated tumor cells were still alive. In addition, the F3-MBI-NP-treated tumor cells were killed only in the area under illumination; in contrast, and as a control, the cells in the area with no illumination stayed alive, indicating that the NPs showed no dark toxicity after 15 min incubation (Fig. 9). Analogous viability changes were also found for the PEG-MBII-NP-treated tumor cells and the F3-MBII-NP-treated cells. After only 1 min illumination, the F3-MBII-NPs killed the MDA-MB-435 tumor cells effectively, under illumination, but showed no cytotoxicity under dark conditions.

Dark toxicity

The dark toxicity effect of the MB-PAA NPs on the MDA-MB-435 cells was evaluated by an MTT assay, as shown in Fig. 10. The cell viabilities were over 90% after incubation with MBI-PAA NPs (0.2 mg mL^{-1}) or MBII-PAA NPs (0.2 mg mL^{-1}) for 1 h, respectively. Both kinds of MB-PAA NPs showed no significant cytotoxicity when not under illumination.

Conclusions

Two novel variants of MB-conjugated PAA NPs were synthesized, enabling a high, non-leachable and an optimized photosensitizer loading for high $^1O_2$ production. The prepared MB-conjugated PAA NPs showed significantly lower MB deactivation by enzymes, compared to their respective MB derivatives, giving an expectation of high *in vivo* PDT efficacy. The MB loading amount in these two kinds of NPs was controlled by the input amount, enabling optimization of $^1O_2$ production. The best $^1O_2$ production, for both MBI-NPs and MBII-NPs, was obtained with MB loadings around 11 nmol mg^{-1}. It was found that the highest $^1O_2$ production of the NPs followed the order of MBI-PAA NPs > MBII-PAA NPs > MBSE-PAA NPs > MB-encapsulated PAA NPs. Both MBI-NPs and MBII-NPs were modified by attaching the tumor-targeting ligand, F3 peptide. *In vitro* PDT data showed that both kinds of targeted NPs, F3-MBI-PAA-NPs and F3-MBII-PAA-NPs, killed tumor cells effectively, with only 1 min illumination, in contrast to the same NPs with no F3. None of the NPs, targeted and untargeted, showed dark toxicity. We believe that our current work will contribute towards further applications of MB in photodynamic therapy.

Acknowledgments

This work was supported by grants R01 EB007977 and R01 EB007977-02s1 (RK) and, in part, by R33CA125297 and R33CA125297-03s1 (RK). We acknowledge the staff of the Electron Microscopy Analysis Laboratory at the University of Michigan.

Notes and references

1. Buytaert E, Dewaele M, Agostinis P. Molecular effectors of multiple cell death pathways initiated by photodynamic therapy. Biochim Biophys Acta, Rev Cancer. 2007; 1776:86–107.
2. Siegel MM, Tabei K, Tsao RS, Pastel MJ, Pandey RK, Berkenkamp S, Hillenkamp F, de Vries MS. Comparative mass spectrometric analyses of photofrin oligomers by fast atom bombardment mass spectrometry, UV and IR matrix-assisted laser desorption ionization mass spectrometry, electrospray ionization mass spectrometry and laser desorption/jet-cooling photoionization mass spectrometry. J Mass Spectrom. 1999; 34:661–669. [PubMed: 10394631]
3. Dolmans DEJGJ, Fukumura D, Jain RK. Photodynamic therapy for cancer. Nat Rev Cancer. 2003; 3:380–387. [PubMed: 12724736]
4. Brown SB, Brown EA, Walker I. The present and future role of photodynamic therapy in cancer treatment. Lancet Oncol. 2004; 5:497–508. [PubMed: 15288239]
5. Wilson BC, Patterson MS. The physics, biophysics and technology of photodynamic therapy. Phys Med Biol. 2008; 53:R61–R109. [PubMed: 18401068]
6. Juarranz A, Jaen P, Sanz-Rodriguez F, Cuevas J, Gonzalez S. Photodynamic therapy of cancer. Basic principles and applications. Clin Transl Oncol. 2008; 10:148–154. [PubMed: 18321817]
7. Bechet D, Couleaud P, Frochot C, Viriot ML, Guillemin F, Barberi-Heyob M. Nanoparticles as vehicles for delivery of photodynamic therapy agents. Trends Biotechnol. 2008; 26:612–621. [PubMed: 18804298]
8. Trindade GS, Farias SLA, Rumjanek VM, Capella MAM. Methylene blue reverts multidrug resistance: sensitivity of multidrug resistant cells to this dye and its photodynamic action. Cancer Lett. 2000; 151:161–167. [PubMed: 10738110]
9. Mellish KJ, Cox RD, Vernon DI, Griffiths J, Brown SB. In vitro photodynamic activity of a series of methylene blue analogues. Photochem Photobiol. 2002; 75:392–397. [PubMed: 12003129]
10. Gabrielli D, Belisle E, Severino D, Kowaltowski AJ, Baptista MS. Binding, aggregation and photochemical properties of methylene blue in mitochondrial suspensions. Photochem Photobiol. 2004; 79:227–232. [PubMed: 15115294]
11. Bongard RD, Merker MP, Shundo R, Okamoto Y, Roerig DL, Linehan JH, Dawson CA. Reduction of thiazine dyes by bovine pulmonary arterial endothelial-cells in culture. Am J Physiol. 1995; 13:L78–L84. [PubMed: 7631818]
12. Umbreit J. Methemoglobin—It's not just blue: A concise review. Am J Hematol. 2007; 82:134–144. [PubMed: 16986127]
13. Wainwright M. Non-porphyrin photosensitizers in biomedicine. Chem Soc Rev. 1996; 25:351–359.
14. Sharman WM, Allen CM, van Lier JE. Photodynamic therapeutics: basic principles and clinical applications. Drug Discovery Today. 1999; 4:507–517. [PubMed: 10529768]
15. Tuite EM, Kelly JM. Photochemical Interactions of Methylene-Blue and Analogs with DNA and Other Biological Substrates. J Photochem Photobiol, B. 1993; 21:103–124. [PubMed: 8301408]
16. Orth K, Russ D, Beck G, Ruck A, Beger HG. Photochemotherapy of experimental colonic tumours with intra-tumorally applied methylene blue. Langenbecks Arch Surg. 1998; 383:276–281. [PubMed: 9776456]
17. Orth K, Rück A, Stanescu A, Beger HG. Intraluminal treatment of inoperable oesophageal tumours by intralesional photodynamic therapy with methylene blue. Lancet. 1995; 345:519–520. [PubMed: 7532255]
18. Orth K, Beck G, Genze F, Ruck A. Methylene blue mediated photodynamic therapy in experimental colorectal tumors in mice. J Photochem Photobiol, B. 2000; 57:186–192. [PubMed: 11154085]

19. May JM, Qu ZC, Cobb CE. Reduction and uptake of methylene blue by human erythrocytes. Am J Physiol: Cell Physiol. 2004; 286:C1390–C1398. [PubMed: 14973146]
20. Porkka K, Laakkonen P, Hoffman JA, Bernasconi M, Ruoslahti E. A fragment of the HMGN2 protein homes to the nuclei of tumor cells and tumor endothelial cells in vivo. Proc Natl Acad Sci U S A. 2002; 99:7444–7449. [PubMed: 12032302]
21. Christian S, Pilch J, Akerman ME, Porkka K, Laakkonen P, Ruoslahti E. Nucleolin expressed at the cell surface is a marker of endothelial cells in angiogenic blood vessels. J Cell Biol. 2003; 163:871–878. [PubMed: 14638862]
22. Maeda H. The enhanced permeability and retention (EPR) effect in tumor vasculature: The key role of tumor-selective macromolecular drug targeting. Adv Enzyme Regul. 2001; 41:189–207. [PubMed: 11384745]
23. Tang W, Xu H, Kopelman R, Philbert MA. Photodynamic characterization and in vitro application of methylene blue-containing nanoparticle platforms. Photochem Photobiol. 2005; 81:242–249. [PubMed: 15595888]
24. Harrel JA, Kopelman R. Biocompatible probes measure intra-cellular activity. Biophotonics Int. 2000; 7:22–24.
25. Xu H, Buck SM, Kopelman R, Philbert MA, Brasuel M, Ross BD, Rehemtulla A. Photoexcitation-based nano-explorers: Chemical analysis inside live cells and photodynamic therapy. Isr J Chem. 2004; 44:317–337.
26. Ross B, Rehemtulla A, Koo Y-EL, Reddy R, Kim G, Behrend C, Buck S, Schneider RJ, Philbert MA, Weissleder R, Kopelman R. Photonic and magnetic nanoexplorers for biomedical use: from subcellular imaging to cancer diagnostics and therapy. Proc SPIE. 2004; 5331:76–83.
27. Kopelman R, Koo Y-EL, Philbert M, Moffat BA, Reddy GR, McConville P, Hall DE, Chenevert TL, Bhojani MS, Buck SM, Rehemtulla A, Ross BD. Multifunctional nanoparticle platforms for in *vivo* MRI enhancement and photodynamic therapy of a rat brain cancer. J Magn Magn Mater. 2005; 293:404–410.
28. Reddy GR, Bhojani MS, McConville P, Moody J, Moffat BA, Hall DE, Kim G, Koo Y-EL, Woolliscroft MJ, Sugai JV, Johnson TD, Philbert MA, Kopelman R, Rehemtulla A, Ross BD. Vascular targeted nanoparticles for imaging and treatment of brain tumors. Clin Cancer Res. 2006; 12:6677–6686. [PubMed: 17121886]
29. Koo Y-EL, Reddy GR, Bhojani M, Schneider R, Philbert MA, Rehemtulla A, Ross BD, Kopelman R. Brain cancer diagnosis and therapy with nanoplatforms. Adv Drug Delivery Rev. 2006; 58:1556–1577.
30. Peer D, Karp JM, Hong S, Farokhzad OC, Margalit R, Langer R. Nanocarriers as an emerging platform for cancer therapy. Nat Nanotechnol. 2007; 2:751–760. [PubMed: 18654426]
31. Davis ME, Chen Z, Shin DM. Nanoparticle therapeutics: an emerging treatment modality for cancer. Nat Rev Drug Discovery. 2008; 7:771–782.
32. Tang W, Xu H, Park EJ, Philbert MA, Kopelman R. Encapsulation of methylene blue in polyacrylamide nanoparticle platforms protects its photodynamic effectiveness. Biochem Biophys Res Commun. 2008; 369:579–583. [PubMed: 18298950]
33. Susa M, Iyer AK, Ryu K, Hornicek FJ, Mankin H, Amiji MM, Duan ZF. Doxorubicinloaded Polymeric Nanoparticulate Delivery System to overcome drug resistance in osteosarcoma. BMC Cancer. 2009; 9:399. [PubMed: 19917123]
34. Chavanpatil MD, Khdair A, Patil Y, Handa H, Mao GZ, Panyam J. Polymer-surfactant nanoparticles for sustained release of water-soluble drugs. J Pharm Sci. 2007; 96:3379–3389. [PubMed: 17721942]
35. Khdair A, Gerard B, Handa H, Mao G, Shekhar MPV, Panyam J. Surfactant-polymer nanoparticles enhance the effectiveness of anticancer photodynamic therapy. Mol Pharmaceutics. 2008; 5:795–807.
36. Khdair A, Handa H, Mao GZ, Panyam J. Nanoparticle-mediated combination chemotherapy and photodynamic therapy overcomes tumor drug resistance in vitro. Eur J Pharm Biopharm. 2009; 71:214–222. [PubMed: 18796331]

37. Hah HJ, Kim G, Koo Lee Y-E, Orringer DA, Sagher O, Philbert MA, Kopelman R. Methylene blue-conjugated hydrogel nanoparticles and tumor-cell targeted photodynamic therapy. Macromol Biosci. 2011; 11:90–99. [PubMed: 20976722]

38. Moreno MJ, Monson E, Reddy RG, Rehemtulla A, Ross BD, Philbert M, Schneider RJ, Kopelman R. Production of singlet oxygen by $Ru(dpp(SO_3)_2)_3$ incorporated in polyacrylamide PEBBLES. Sens Actuators, B. 2003; 90:82–89.

39. Winer I, Wang S, Koo Lee Y-E, Fan W, Gong Y, Burgos-Ojeda D, Spahlinger G, Kopelman R, Buckanovich RJ. F3-targeted cisplatin-hydrogel nanoparticles as an effective therapeutic that targets both murine and human ovarian tumor endothelial cells in vivo. Cancer Res. 2010; 70:8674–8683. [PubMed: 20959470]

40. Carroll MK, Unger MA, Leach AM, Morris MJ, Ingersoll CM, Bright FV. Interactions between methylene blue and sodium dodecyl sulfate in aqueous solution studied by molecular spectroscopy. Appl Spectrosc. 1999; 53:780–784.

41. Patil K, Pawar R, Talap P. Self-aggregation of Methylene Blue in aqueous medium and aqueous solutions of Bu4NBr and urea. Phys Chem Chem Phys. 2000; 2:4313–4317.

42. Ghanadzadeh A, Zeini A, Kashef A, Moghadam M. Concentration effect on the absorption spectra of oxazine1 and methylene blue in aqueous and alcoholic solutions. J Mol Liq. 2008; 138:100–106.

43. Orringer DA, Koo Y-EL, Chen T, Kim G, Hah HJ, Xu H, Wang SY, Keep R, Philbert MA, Kopelman R, Sagher O. In vitro characterization of a targeted, dye-loaded nanodevice for intraoperative tumor delineation. Neurosurgery. 2009; 64:965–971. [PubMed: 19404156]

44. Koo Lee Y-E, Ulbrich EE, Kim G, Hah H, Strollo C, Fan WZ, Gurjar R, Koo SM, Kopelman R. Near infrared luminescent oxygen nanosensors with nanoparticle matrix tailored sensitivity. Anal Chem. 2010; 82:8446–8455. [PubMed: 20849084]

45. van Vlerken LE, Vyas TK, Amiji MM. Poly(ethylene glycol)-modified nanocarriers for tumor-targeted and intracellular delivery. Pharm Res. 2007; 24:1405–1414. [PubMed: 17393074]

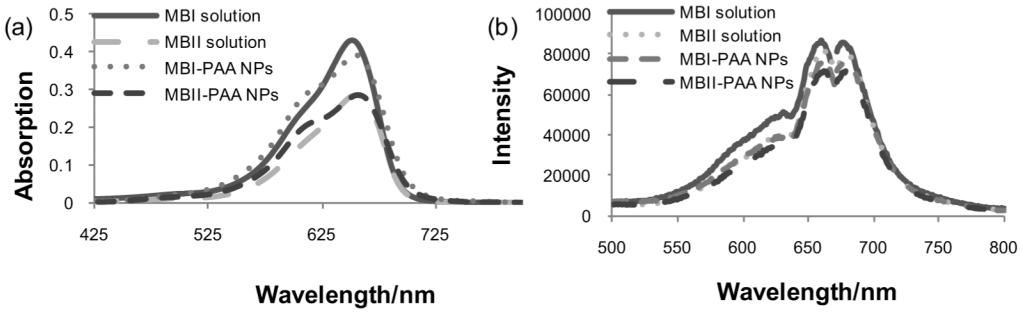

Fig 1.

(a) UV-vis spectra of 1 mg mL^{-1} MBI-PAA NP (MBI loading: 11.0 nmol mg^{-1}), 1 mg mL^{-1} MBII-PAA NP (MB loading: 10.4 nmol mg^{-1}), 11.0 μM MBI and 10.4 μM MBII solutions, when dissolved in DI water. (b) Excitation and emission spectra of 0.3 mg mL^{-1} MBI-PAA NP (MBI loading: 11.0 nmol mg^{-1}), 0.3 mg mL^{-1} MBII-PAA NP (MB loading: 10.4 nmol mg^{-1}), 3.3 μM MBI and 3.1 μM MBII solutions, when dissolved in PBS buffer (pH 7.4).

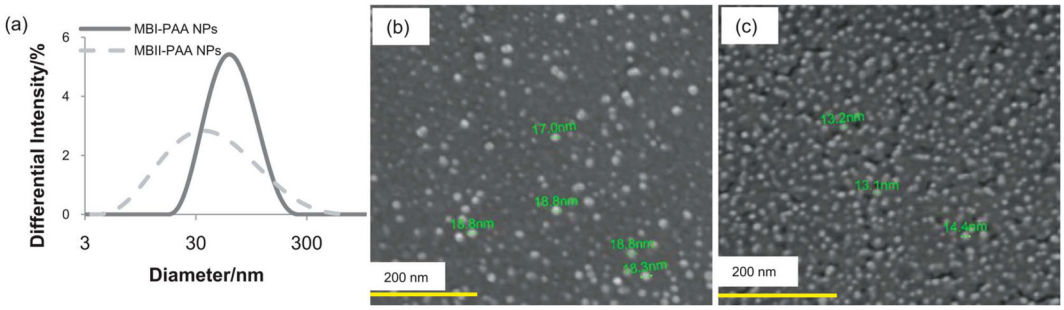

Fig 2.

(a) DLS curves of MBI-PAA NPs (MBI loading: 6.4 nmol mg^{-1}) and MBII-PAA NPs (MBII loading: 10.4 nmol mg^{-1}); (b) SEM image of MBI-PAA NPs (MBI loading: 11.0 nmol mg^{-1}) and (c) SEM image of MBII-PAA NPs (MBII loading: 10.4 nmol mg^{-1}).

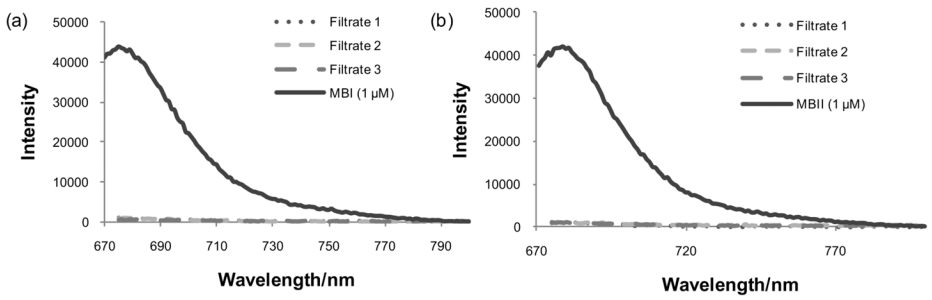

Fig 3.

Fluorescence emission spectra of MB in the filtrates of (a) MBI-PAA NP solution (dye loading: 13.8 nmol mg^{-1}) and (b) MBII-PAA NP solution (dye loading: 12.9 nmol mg^{-1}) after dye leaching test, showing no measurable leaching of MB from the NPs.

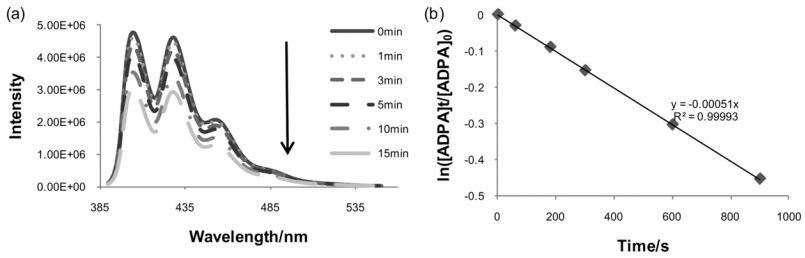

Fig 4.

(a) Fluorescence spectra of ADPA in a mixed PBS buffer solution (pH 7.4) with 0.3 mg mL^{-1} MBII-PAA NP (MBII loading: 10.4 nmol mg^{-1}) solution, after irradiation at 660 nm for 0, 1, 3, 5, 10, and 15 min. (b) Linear fit on the change of ADPA fluorescence intensity at 406 nm to irradiation time, showing the k value of MBII-PAA NPs (MBII loading: 10.4 nmol mg^{-1}) was 5.1×10^{-4} s^{-1}.

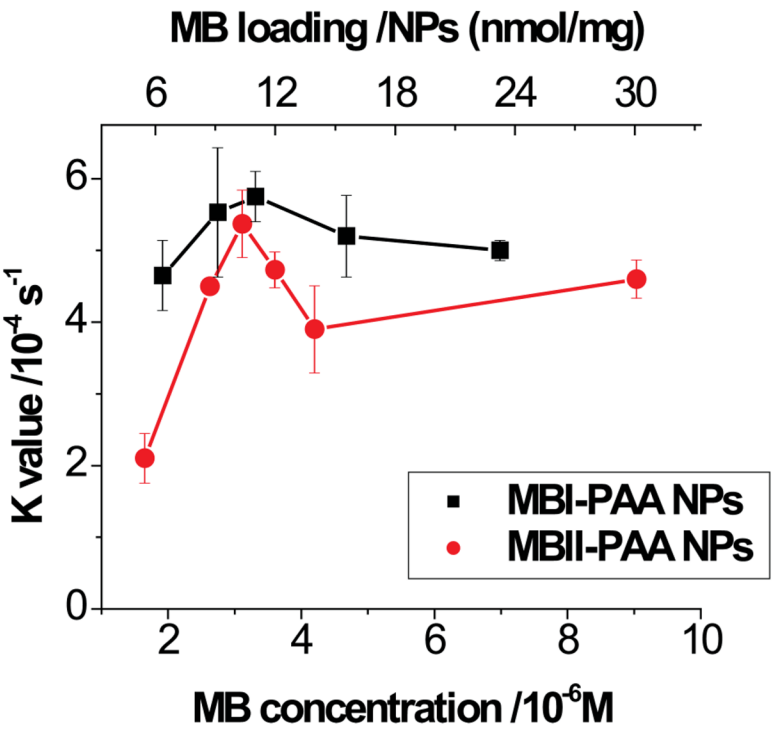

Fig 5.

k value *vs.* MB concentration and MB loading of the NPs in MBI-PAA NPs and MBII-PAA NPs solution (0.3 mg mL^{-1} in PBS buffer).

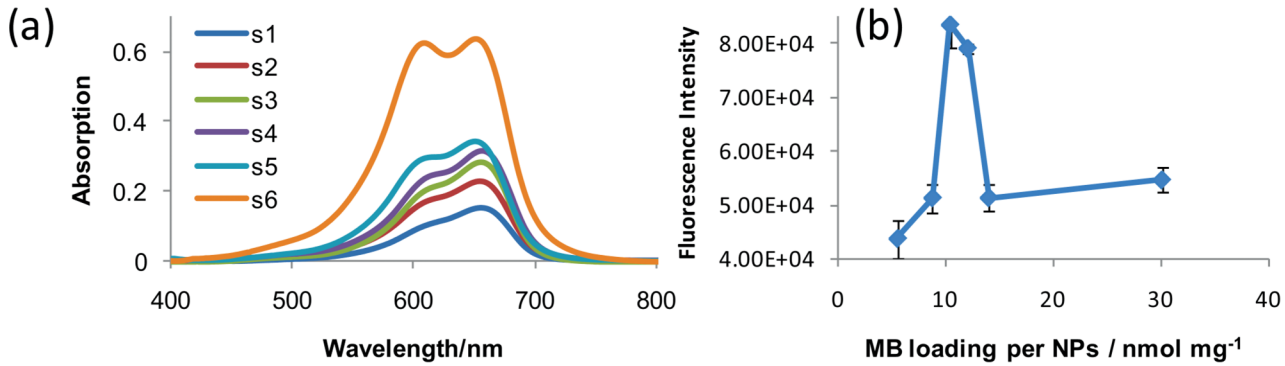

Fig 6.

UV-vis spectra of MBII-PAA NPs (1 mg ml^{-1} in DI water) (a) and fluorescence intensity *vs.* MB loading in MBII-PAA NPs (0.3 $mgml^{-1}$ in PBS buffer, excitation/emission: 660 nm/680 nm) (b). S1 to S6 in (a) are MBII-PAA NPs with MB loading of 5.5 nmol mg^{-1}, 8.7 nmol mg^{-1}, 10.4 nmol mg^{-1}, 12.0 nmol mg^{-1}, 14.0 nmol $mg^{-1}$and 30.1 nmol mg^{-1}, respectively.

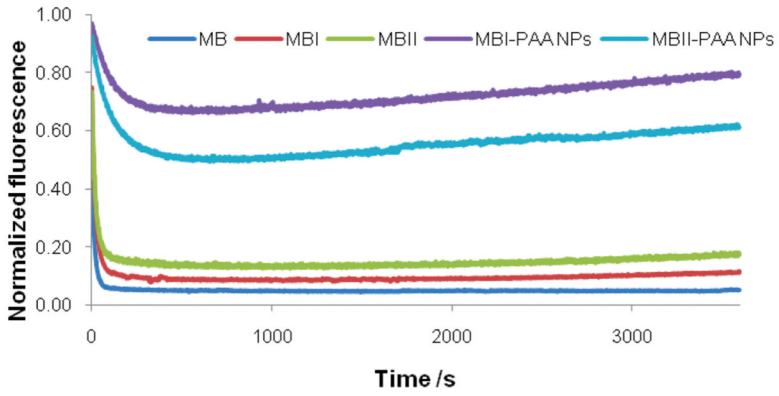

Fig 7.

Enzymatic reduction test results: normalized fluorescence emission intensity at 680 nm of MB (3 μM), MBI (3 μM), MBII (3 μM), MBI-PAA NP (0.3 mg mL^{-1}, dye loading: 11.0 nmol mg^{-1}) and MBII-PAA NP (0.3 mg mL^{-1}, dye loading: 10.4 nmol mg^{-1}) solutions. All samples were dissolved in PBS buffer (pH 7.4), and mixed with 0.45 μmol NADH and 0.05 mg diaphorase. The photobleaching effect of MB was removed from all the curves.

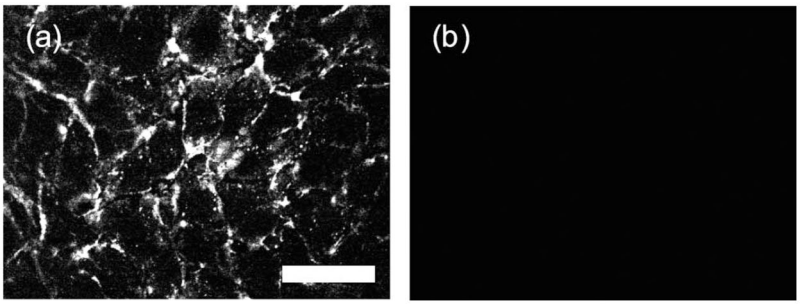

Fig 8.

Confocal microscopy images of MDA-MB-435 cells after 15 min incubation with (a) F3-MBI-PAA NPs and (b) PEG-MBI-PAA NPs. NP concentration: 0.3 mg mL^{-1}; dye loading: 11.0 nmol mg^{-1}; scale bar: 50 μm.

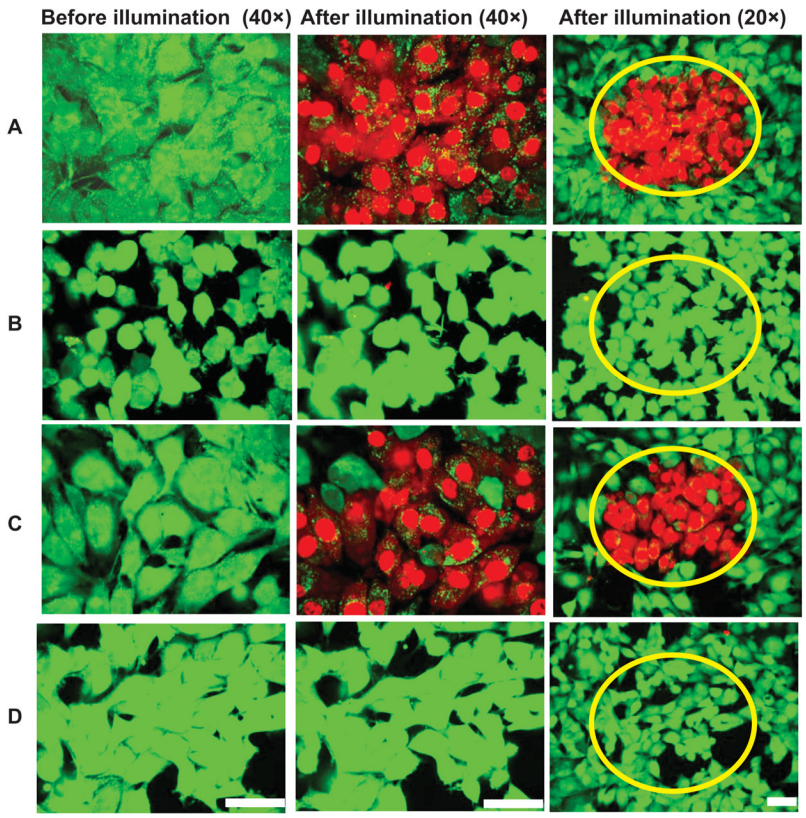

Fig 9.

Confocal microscopy images of MDA-MB-435 cells stained with calcein-AM (green, living cell) and PI (red, dead cell), using a 20× or 40× objective lens, respectively. The cells were incubated with F3-targeted or PEGylated NP solution (0.1 mg mL^{-1} in PBS buffer (pH 7.4)) for 15 min, respectively: (A) F3- MBI-PAA NPs; (B) PEG-MBI-PAA NPs; (C) F3- MBII-PAA NPs; (D) PEG-MBII-PAA NPs. After incubation, the cells were illuminated at 647 nm with 400 μW of power (*ca.* 100 J cm^{-2}) for 1 min. These images were taken before illumination and 20 min after illumination. In the images after illumination (20×), only the cells in the circled central area were illuminated. Scale bar: 50 μm.

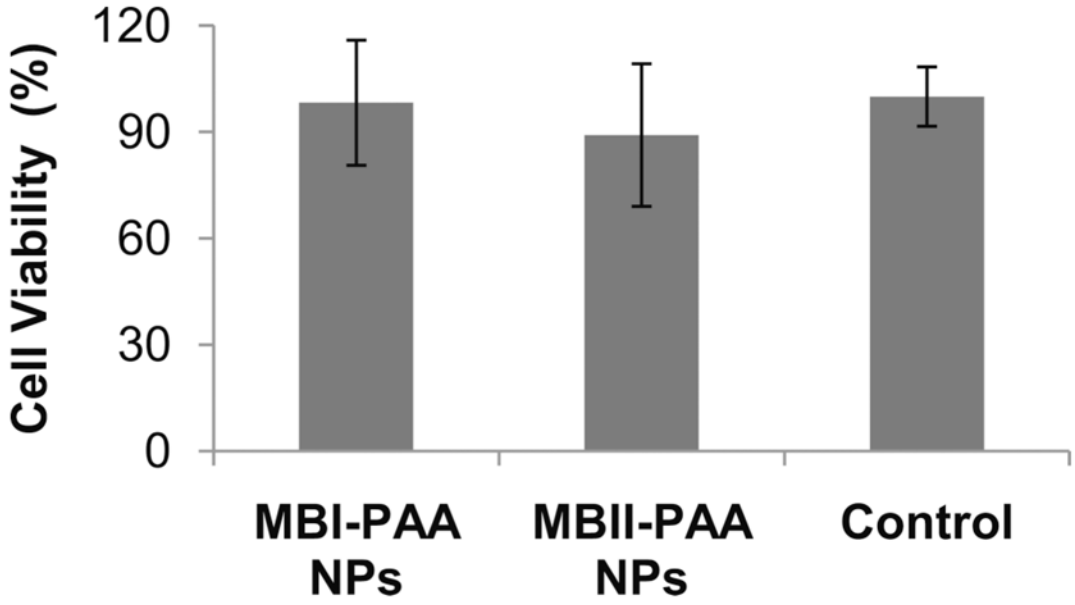

Fig 10.

The viability of MDA-MB-435 cells from MTT assay, after incubation for 1 h with 0.2 mg mL^{-1} MBI-PAA NP solution (dye loading: 11.0 nmol mg^{-1}) and 0.2 mg mL^{-1} MBII-PAA NP solution (dye loading: 10.4 nmol mg^{-1}), respectively. These results showed the dark toxicity of MBI-PAA NPs and MBII-PAA NPs. The average value was obtained from 7 samples. Error bars indicate the standard deviation.

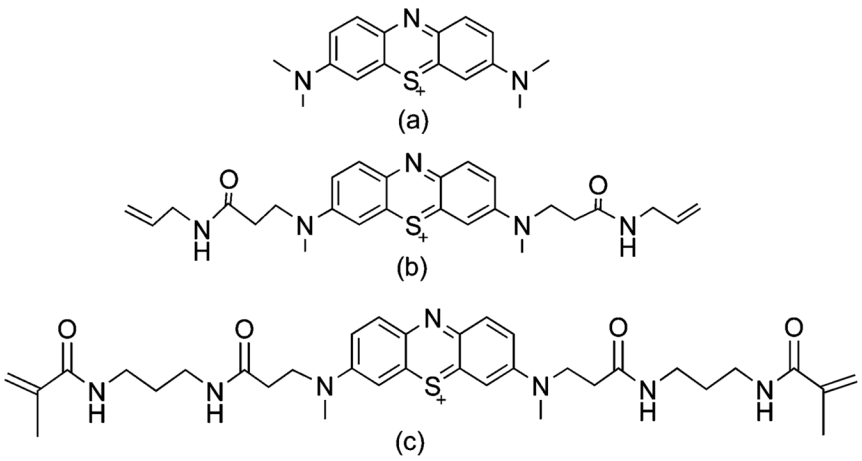

Scheme 1.
Molecular structure of (a) methylene blue (MB), (b) 3, 7-bisallylmethylene blue (MBI), and (c) 3,7-bismethylacrylamide methylene blue (MBII).

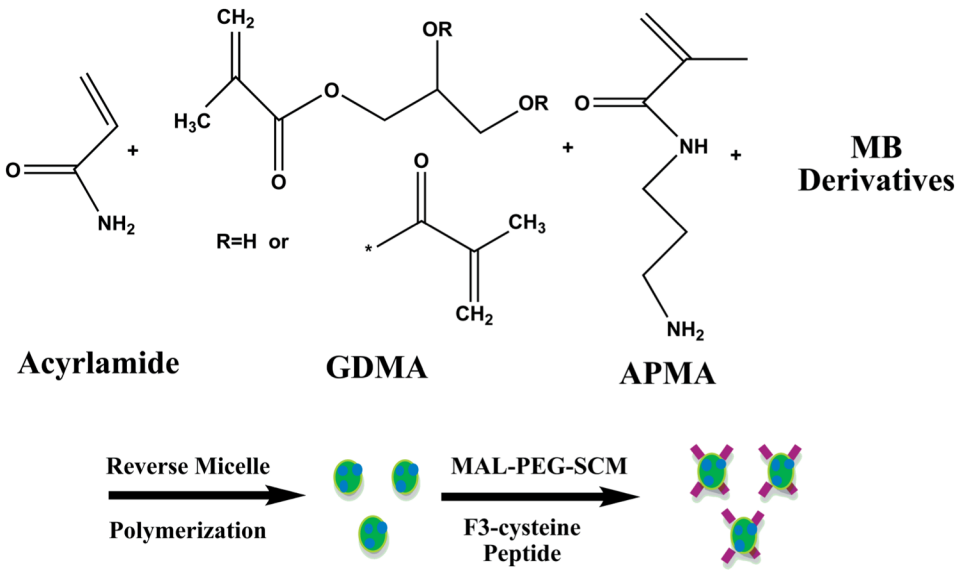

Scheme 2.
Preparation and F3-targeting of polyacrylamide nanoparticles.

Table 1

Best k values of MB-encapsulated NPs, MBSE-PAA NPs, MBI-PAA NPs and MBII-PAA NPs in PBS buffer (pH 7.4)

NPs	MB-encapsulated NPs[23]	MBSE-PAA NPs[37]	MBI-PAA NPs	MBII-PAA NPs
MB loading/NPs (nmol mg^{-1})	3.3	7.7	11.0	10.4
k value (10^{-4} s^{-1})	1.0 ± 0.1	9.3 ± 0.5	20.1 ± 1.5	16.3 ± 1.4

The *k* values above are for the NP solutions of 1 mg mL^{-1}. The *k* values of MBI-PAA NPs and MBII-PAA NPs at 1 mg mL^{-1} were converted from those at 0.3 mg mL^{-1} using eqn (2) and absorbance values of the NP solutions at 0.3 and 1 mg mL^{-1}.